Journal of
Ship&Ocean
Technology
© JUNE 1999

SOTECH Vol.3, No.2; pp.1~16

Influence of Leading Edge Radii on Hydrodynamic Performances of a Foil Section

Jong-Woo Ahn, Il-Sung Moon, Jin-Tae Lee

Korea Research Institute of Ships and Ocean Engineering, Taejon, Korea

Abstract

The incompressible Reynolds-Averaged Navier-Stokes(RANS) equations are solved using the standard $k-\epsilon$ turbulence model and a finite volume method(FVM) with an O-type grid system. The computed results for its performance test are in good agreement with the published experimental data. The present method is applied to the study on the leading edge radius of a hydrofoil section. Calculated results suggest that the leading edge radius has some effects on cavitation performances of a 2-D foil. A natural leading edge radius for the NACA66 section is determined from this study.

Keywords : L. E. radius, FVM, O-type grid, Standard $k-\epsilon$ turbulence model

1 Introduction

Marine propellers usually operate in complicate non-uniform wake fields at ship's stern ends. Due to non-uniform wakes, the blade sections of marine propellers encounter a wide range of angles of attack. Moreover the onset flows to propellers are highly turbulent.

In a practical marine propeller design process, the NACA66 thickness form(TMB mod.) and the $a = 0.8$ mean line (hereafter referred to as the NACA66 foil) are commonly adopted, which have been originally developed for airfoil applications. However, aircraft wings usually operate in uniform flows with relatively low turbulent intensities and with no risk of cavitation. Due to these different operating conditions between marine propellers and aircraft wings, special considerations should be taken into account for the development of propeller blade sections, such as having better hydrodynamic performances in a wide range of angles of attack.

A foil section is usually defined as a set of section ordinates at specified chordwise locations. Foil geometry is generated by interpolating the section ordinates. The detailed leading edge shape is determined by specifying the leading edge radius. Leading edge shapes can give noticeable influence on the hydrodynamic performances of a foil, especially at higher angle of attack conditions. Moreover adequate leading edge radius is important for natural drawing and manufacturing of a foil.

In the present study, a code for the computation of the flow around two-dimensional foils is developed to investigate the influence of leading edge radii on hydrodynamic characteristics of a foil. The code solves the incompressible RANS equations with the standard $k-\epsilon$ turbulence model. A finite volume method was employed with an O-type grid system. The same grid system at 0° angle of attack was employed for calculation of the flow at different angles of attack, instead

of generating new grid systems corresponding to the different angles of attack, in order to save efforts to regenerate new grid systems. To validate the numerical reliability, the computed results were compared with the published experimental data of Nakayama[Nakayama, 1985] and the experimental results performed at the cavitation tunnel of Korea Research Institute of Ship & Ocean Engineering(KRISO).

The NACA66 sections having specified thickness-chord and camber-chord ratios with different leading edge radii were selected for the study of the influence of leading edge radii. The study reveals that the influence becomes noticeable as angle of attack increases, while that is negligible at near the ideal angle of attack for the computed case. The value for the leading edge radius is newly selected as the most natural value for drawing and manufacturing of the NACA66 section.

2 Governing Equations and Numerical Method

2.1 Governing Equations

For a steady, incompressible turbulent flow, the governing equations can be written in a Cartesian tensor notation as:

$$\frac{\partial U_i}{\partial x_i} = 0, \tag{1}$$

$$U_j \frac{\partial U_i}{\partial x_j} = -\frac{1}{\rho}\frac{\partial P}{\partial x_i} + \frac{\partial}{\partial x_j}\left[\nu \frac{\partial U_i}{\partial x_j} - \overline{u_i u_j}\right], \tag{2}$$

where U_j and u_j are the j-th components of the mean and fluctuating velocities, respectively. P is the mean pressure, ρ and ν are the fluid density and kinematic viscosity. The unknown Reynolds stress $-\overline{u_i u_j}$ can be expressed, by using the concept of eddy viscosity ν_t:

$$-\overline{u_i u_j} = \nu_t \left(\frac{\partial U_i}{\partial x_j} + \frac{\partial U_j}{\partial x_i}\right) - \frac{2}{3} k \delta_{ij} \tag{3}$$

The transport equations for turbulence closure are the equations for the turbulent kinetic energy k and the rate of kinetic energy dissipation ϵ, i.e.,

$$U_j \frac{\partial k}{\partial x_j} = \frac{\partial}{\partial x_j}\left[\left(\nu + \frac{\nu_t}{\sigma_k}\right)\frac{\partial k}{\partial x_j}\right] + P_k - \epsilon, \tag{4}$$

$$U_j \frac{\partial \epsilon}{\partial x_j} = \frac{\partial}{\partial x_j}\left[\left(\nu + \frac{\nu_t}{\sigma_\epsilon}\right)\frac{\partial \epsilon}{\partial x_j}\right] + \frac{\epsilon^2}{k}\left(C_{\epsilon 1}\frac{P_k}{\epsilon} - C_{\epsilon 2}\right) \tag{5}$$

In the above equations, σ_k , σ_ϵ , $C_{\epsilon 1}$ and $C_{\epsilon 2}$ are the model constants. The production of turbulent energy P_k is defined as $P_k \equiv -\overline{u_i u_j}\partial U_i/\partial x_j$ which represents the production due to the shear strain and the normal strain.

$$P_k = \nu_t \left[2\left(\left(\frac{\partial U}{\partial x}\right)^2 + \left(\frac{\partial V}{\partial y}\right)^2\right) + \left(\frac{\partial U}{\partial y} + \frac{\partial V}{\partial x}\right)^2\right] \tag{6}$$

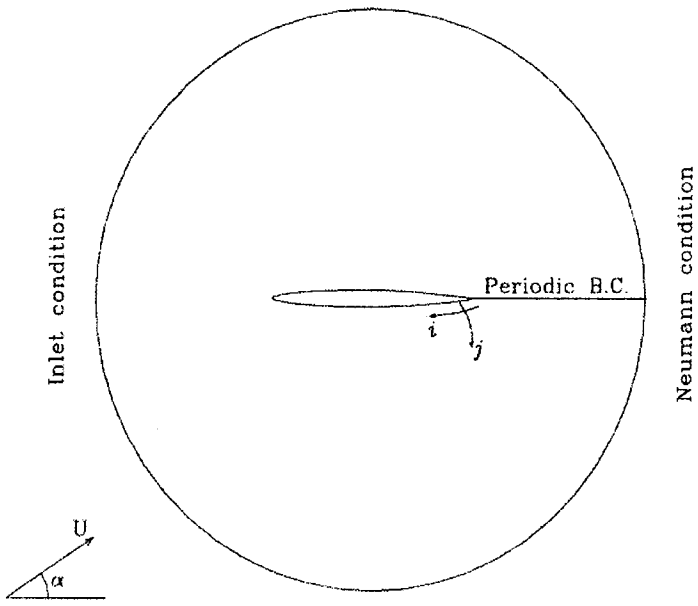

Figure 1. Boundary condition.

2.2 Numerical Method and Boundary Conditions

The differential equations governing the mean and turbulent flowfields are solved numerically by the well-established finite volume method[Rhie et al., 1983]. In this study, the non-orthogonal finer-resolution grid systems are adopted, where the grid points are crowded near the wall boundaries. A non-staggered variable arrangement is adopted with the momentum interpolation technique to avoid the pressure-velocity decoupling. The coupling between pressure and velocity is achieved by the SIMPLEC predictor-corrector algorithm, which is an improved version of the SIMPLE algorithm. The convection terms in U, V, k and ϵ equations are discretized using the hybrid linear and parabolic approximation(HLPA) scheme with second-order accuracy. The set of discretized equations is solved by the periodic tridiagonal matrix algorithm(TDMA). Convergence is declared if the absolute sum of non-dimensional residuals of each governing equation throughout the computation domain is less than 10^{-5}. All the calculations were performed on a Pentium PC. A typical CPU time was approximately 40 minutes for the perfomance analysis of a foil at a given angle of attack. Details regarding the numerical procedure can be found in Ahn et al.[Ahn et al., 1995].

A typical solution domain and boundary conditions are shown in Figure 1. Turbulent flow is assumed for the whole fluid domain. The Neumann boundary conditions for all variables are applied at the outlet. The periodic boundary condition(periodic TDMA) is located from the foil trailing edge to the center of the outlet in the O-type grid sytem. The no-slip boundary conditions are employed on the foil surface: $U = V = k = 0$, $\epsilon_w = \nu \partial^2 k / \partial y^2$ and $\partial P / \partial y = 0$. The calculation of the near-wall region is carried out by bridging the viscosity-affected near-wall layers expressed by a wall function. The first grid point away from the wall is placed outside the viscous layer. The y_p^+ values at the first grid points are within $y_p^+ = 30 \sim 60$ in the present computations.

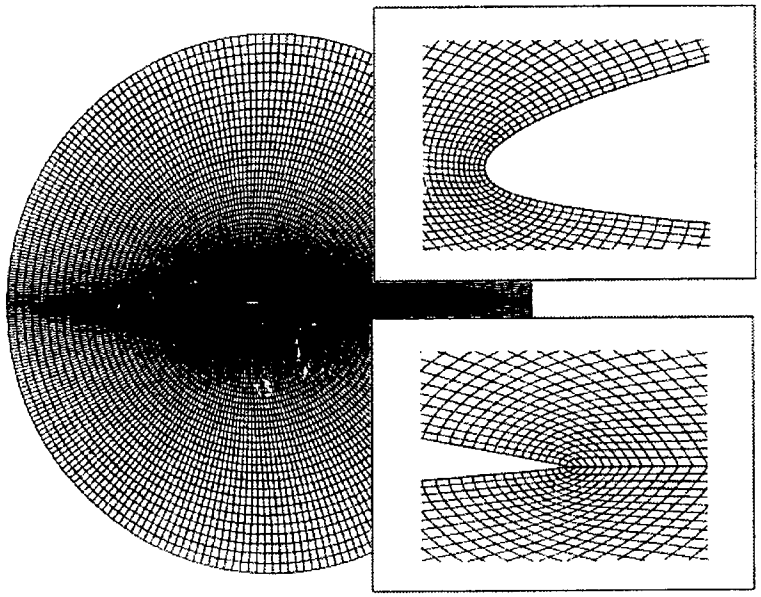

Figure 2. Typical O-type grid system.

An O-mesh is used for the present simulations(Figure 2). A C-mesh is ideally suited for simulating wake flows since better streamwise resolution can be selectively provided in the wake regions. The use of a C-mesh also allows the accurate resolution of a leading edge and boundary layer on the body surface. However, if C-type mesh was to be used for the present simulations, the flow in the region of the wake flows would experience numerical instabilities due to the branch cut. To avoid these instabilities, the momentum interpolation method should be employed and the grid should be reconstructed in such a way that the constant lines passing through all points along the branch-cut are orthogonal to the branch-cut. In the present simulations, several angles of attack will be tested, in which the corresponding grid generations themselves are tedious and time-consuming. Thus, the use of an O-mesh is necessary for obtaining a good solution for several angles of attack.

3 Validation of the Code

3.1 Grid System

An O-type mesh is used for the present calculations(Figure 2). It is important to ascertain the grid independence of the computation results and to validate the accuracy of the present method. An algebraic grid as an initial grid is firstly generated and then an elliptic grid system is generated by solving elliptic partial differential equations. A typical grid system is illustrated in Figure 2, which shows the detailed grids around the leading edge and the trailing edge. The first grid point away from the wall is placed outside the viscous sublayer. The outer boundary is located at $7.0c$ from the trailing edge of foil, where c is the chord length of the foil. Computations are carried out

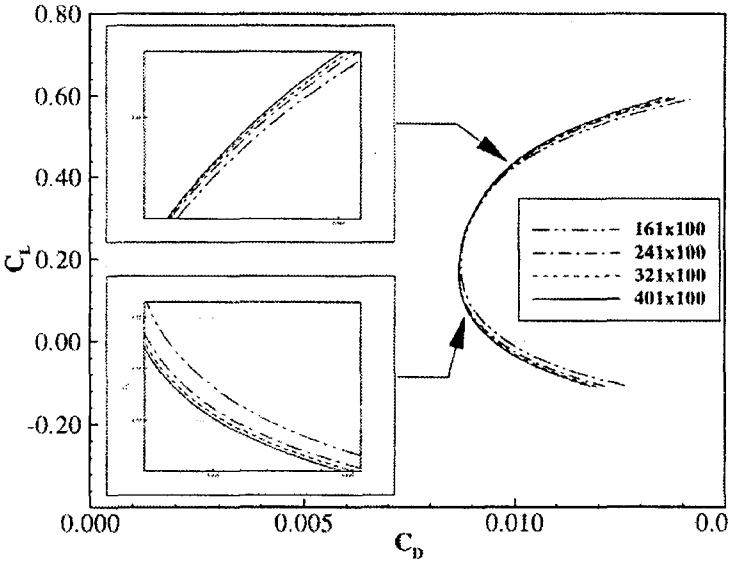

Figure 3. Grid dependence evaluation.

with four different grid systems, i.e., (161 × 100) nodes, (241 × 100) nodes, (321 × 100) nodes and (401 × 100) nodes. The Reynolds number based on the chord length is $Re = 3.0 \times 10^6$.

Comparison of foil performances is presented in Figure 3, where lift and drag are calculated by integrating the surface pressure and skin friction distributions. It is regarded that the convergence of solution is established with (321 × 100) nodes.

3.2 Comparison with Nakayama's Results

To validate the present method, we applied the method for two Nakayama's airfoils[Nakayama, 1985]: one is a 10 %-thick conventional airfoil(DSMA661) and the other is a 14 %-thick advanced supercritical airfoil(DSMA671). In the experiment, DSMA661 was located at the centerline of a wind tunnel at zero angle of attack, while DSMA671 was tested at a geometric angle of attack of 4°. The Reynolds number based on the chord length is 1.2×10^6. The computed surface pressure distributions(C_P) are compared with experiments in Figure 4 for two cases. As shown in Figure 4, the numerical results are in excellent agreement with the experiments. Figure 5 shows the skin friction coefficients(C_f) for the two cases. Although a small discrepancy is detected in the upper surface, the present method can be applied to predict the performance of two dimensional foil sections.

3.3 Comparison with KRISO Results

Lift and drag forces are calcualted by integrating x-component and y-component of the pressure distribution and the skin friction, respectively. Computed lift and drag forces are compared with experimental values performed at the cavitation tunnel in KRISO (Korea Research Institute of Ship and Ocean Engineering). The NACA66 foil section of 0.2m chord length having aspect ratio of

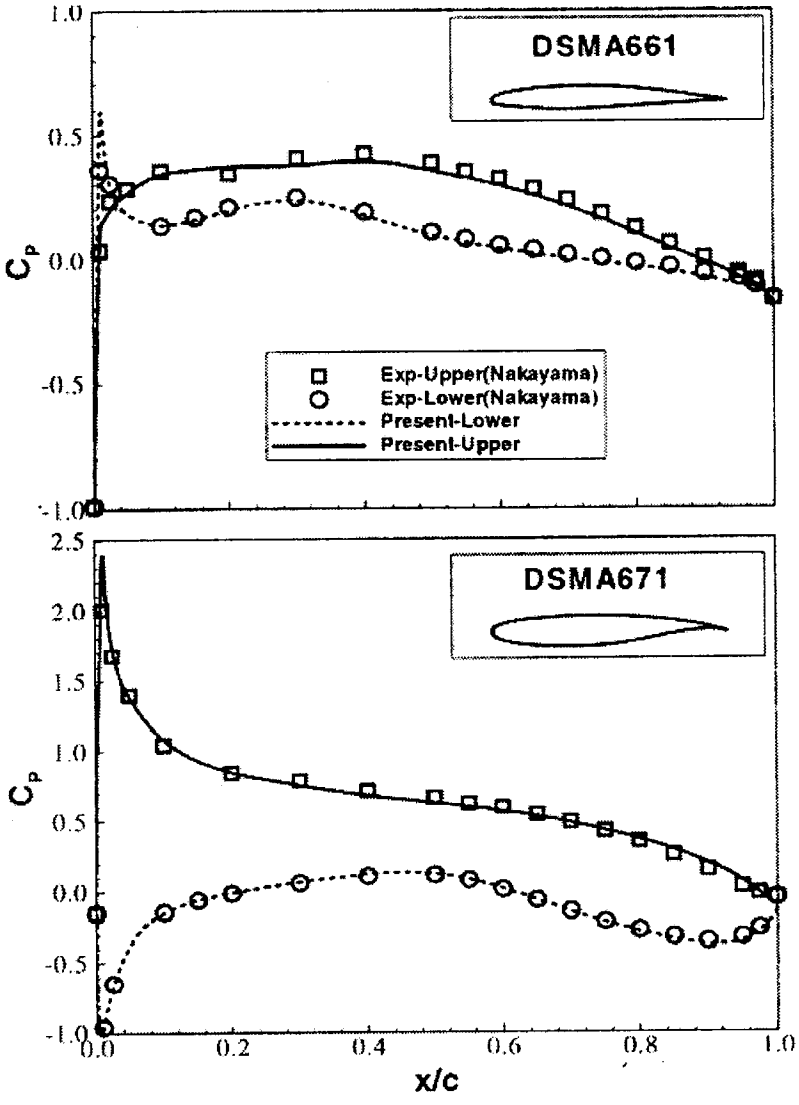

Figure 4. Comparison of the predicted C_p with the experiment.

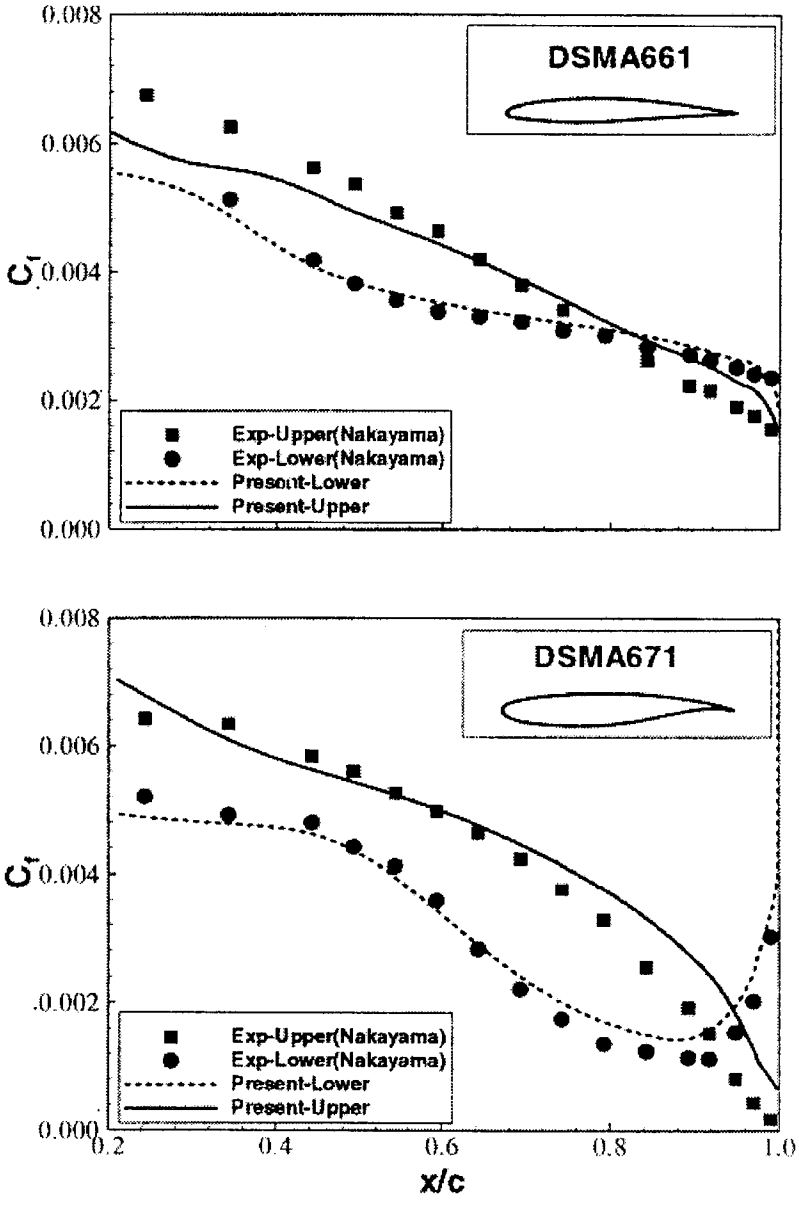

Figure 5. Comparison of the predicted C_f with the experiment.

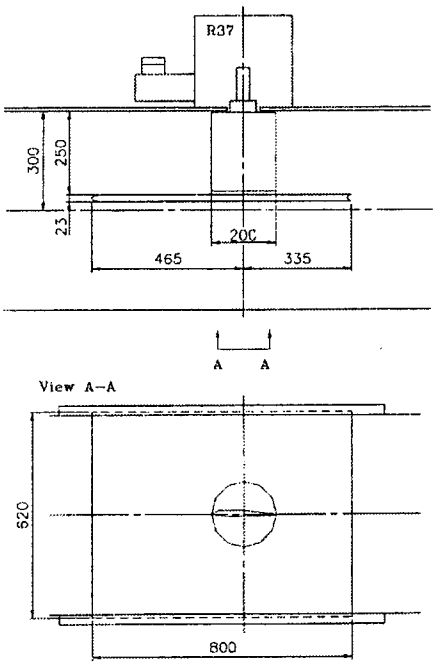

Figure 6. The modified section for the performance test of a 2-D foil.

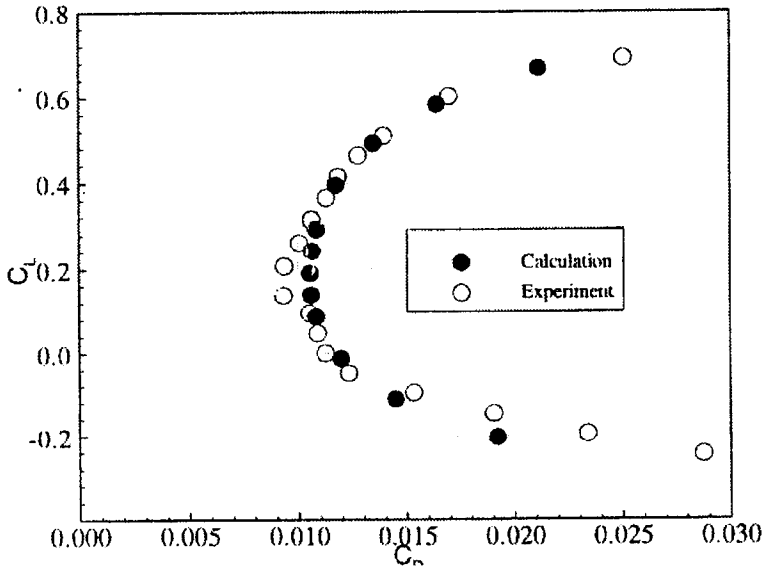

Figure 7. Comparison of the predicted result with the experiment(NACA66).

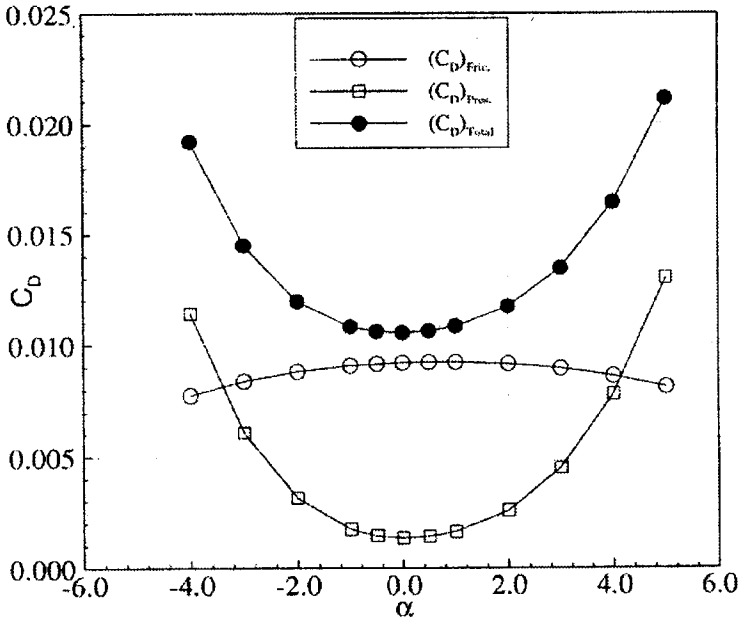

Figure 8. Component of the drag force.

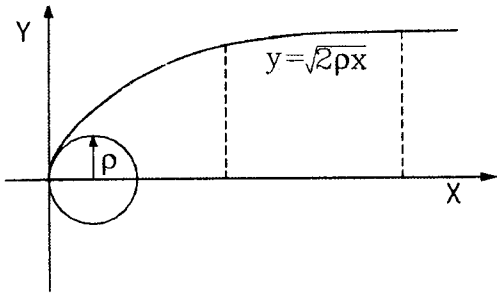

Figure 9. An osculating parabola and a circle at the leading edge.

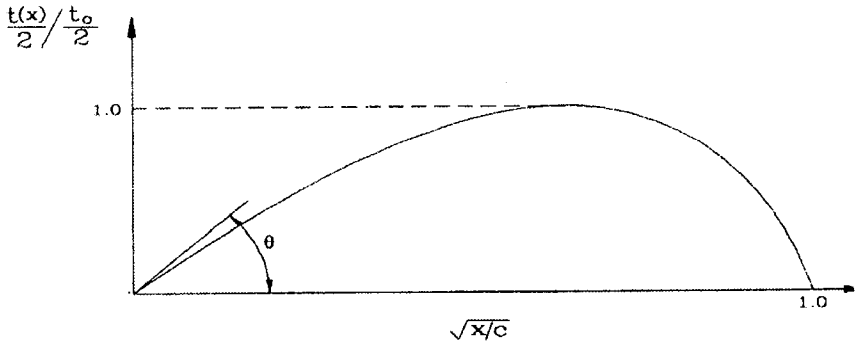

Figure 10. Cubic spline fitting of the thickness ordinates.

1.25 is located in a confined channel flow for the simulation of two-dimensional flow. The leading edge radius coefficient(= $(\rho/c)/(t/c)^2$) is 0.642. An experimental set-up of the foil section in the cavitation tunnel is presented in Figure 6. A six-components balance is installed to measure the forces and moments on the foil section. The Reynolds number based on the chord length is $Re = 1.0 \times 10^6$. In order to stimulate the turbulence on the foil surface, the sand with the 63 μm grain size is attached at 5 % chord position[Park et al., 1998].

The grid size for numerical calculation is 321×100. The angles of attack(α) are -4.0, -3.0, -2.0, -1.0, -0.5, 0.0, 0.5, 1.0, 2.0, 3.0, 4.0 and 5.0. The predicted computational results are compared in Figure 7 with the experimental data. Although slight over-prediction of drag force are seen, the computed lift-drag forces by the present numerical method are in good agreement with the experiment.

Contribution of drag components to the total drag is shown in Figure 8. The drag force can be divided into the skin friction drag and the form drag. While the form drag increases rapidly as the angle of attack(α) increases, the skin friction drag decreases slightly. The slight decrease of the skin friction at higher angle of attack is caused by relatively small velocity gradient near the trailing edge. The total drag curve has the similar trend as the form drag.

4 Leading Edge Radius

4.1 Definition of Leading Edge Radius

Leading edge radius is an important parameter not only for the hydrodynamic performances of hydrofoils, such as cavitation inception[Van gunsteren et al., 1973] and lift-drag characteristics, but also for the easiness of hydrofoil manufacturing. To determine the leading edge radius mathematically[Lee et al., 1988], the thickness distribution near the leading edge is assumed as an osculating parabola around a circle with the leading edge radius ρ, and then the leading edge radius is determined by matching the parabola with the given section offsets(shown in Figure 9). The mathmatical way is described in the following.

For a foil section without camber, the half thickness distribution near the leading edge can be assumed as(shown in Figure 10):

$$y = \sqrt{2\rho x}, \quad for \quad x \ll 1 \tag{7}$$

where ρ is leading edge radius. Equation (7) can be expressed in a non-dimensional form,

$$Y = \sqrt{8\, C_{LER}\, X}\,, \tag{8}$$

where $Y = \frac{y}{t_0/2}$, $X = \frac{x}{c}$ and $C_{LER} = \frac{(\rho/c)}{(t_0/c)^2}$

C_{LER} is the leading edge radius coefficient and is 0.5 for elliptic sections. Generally a thickness form of a foil can be expressed as a cubic function in $\sqrt{X}$,

$$Y = as + bs^2 + cs^3, \tag{9}$$

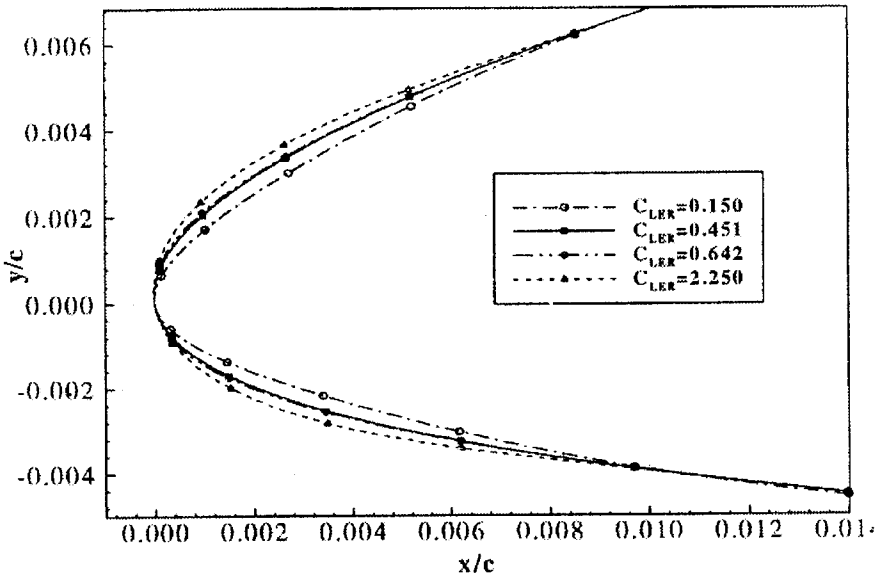

Figure 11. Comparison of the leading edge blow-up geometries.

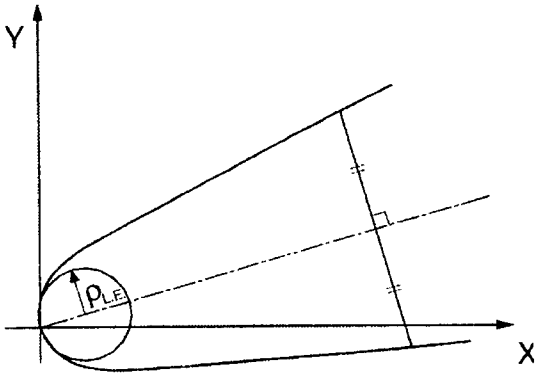

Figure 12. Generation of a cambered foil.

where $s = \sqrt{X}$, and a is the slope of the section ordinates at the leading edge with respect to $\sqrt{X}$. From Equations (8) and (9), we can find the following relation for $x \ll 1$,

$$a = \sqrt{8\, C_{LER}}, \tag{10}$$

and the leading edge radius coefficient can be expressed as:

$$C_{LER} = \frac{\rho/c}{t_o/c} = \frac{a^2}{8} \tag{11}$$

Foil geometry is generated by interpolating the given offset values using a cubic spline routine. The cubic spline routine assumes that the foil geometry is expressed as a piecewise cubic function of $\rho = \sqrt{x/c}$ between the given chordwise locations and the slopes at the chordwise locations are continuous. However, since the detailed geometry near the leading edge is not uniquely determined for a given set of section ordinates, the geometry can be generated with various leading edge slopes, which are related with the leading edge radius coefficients.

A natural way to determine the leading edge radius is that the thickness ordinates be interpolated with the cubic spline routine and the slope at the leading edge be calculated as the output of the routine, to be $a = dY/ds = tan\theta$, as shown in Figure 10. Then the leading edge radius coefficient C_{LER} can be calculated from Eq. (11).

Figure 11 shows blow-up drawings of the foil geometries near the leading edge with different C_{LER} of 0.150, 0.451, 0.642 and 2.250. The C_{LER} of 0.150 and 2.250 are the minimum and maximum values, with which smooth foil geometries passing through the given thickness ordinates can be generated. The value of 0.642 has been used at KRISO. However, propeller manufacturers sometimes argued that the value is somewhat big for manufacturing of propellers with the NACA66 section. The value of 0.451 is considered to be the most suitable value to draw and manufacture NACA66 sections.

The thickness distribution is superposed at the right angle on a given camber line, as shown in Figure 12, to generate the geometry of a cambered foil.

4.2 Hydrodynamic Characteristics of NACA66 Foils with Different Leading Edge Radii

Computations were performed at $Re = 3.0 \times 10^6$, using the code described in Section 2, for a NACA66 section with maximum thickness-chord ratio(t_o/c) of 0.0571 and maximum camber-chord ratio(f_o/c) of 0.0168, which are typical values for a marine propeller blade section at 0.7 radius. Detailed leading edge shapes were varied by adopting different non-dimensional leading edge radii(ρ/c) of 0.49×10^{-3}, 1.47×10^{-3}, 2.09×10^{-3} and 7.34×10^{-3}, which correspond to the leading edge radius coefficients of 0.150, 0.451, 0.642 and 2.250, respectively.

Lift-drag characteristics and pressure distributions on the foil surface at various angles of attack were computed. Figure 13 shows the lift-drag characteristics of the foils with various leading edge radii. Effect of leading edge radii on the lift-drag curves is negligible at near the ideal angle of attack since the slight difference of the leading edge geometry does not give significant effects on lift and drag values. As the attack angle increases, influence of the leading edge radius becomes noticeable. A larger leading edge radius foil has lower drag coefficient for the same lift coefficient, and as a result, gives a wider lift-drag curve. C_{LER} value change from 0.451 to 0.642 gives negligible influence on the lift-drag curves.

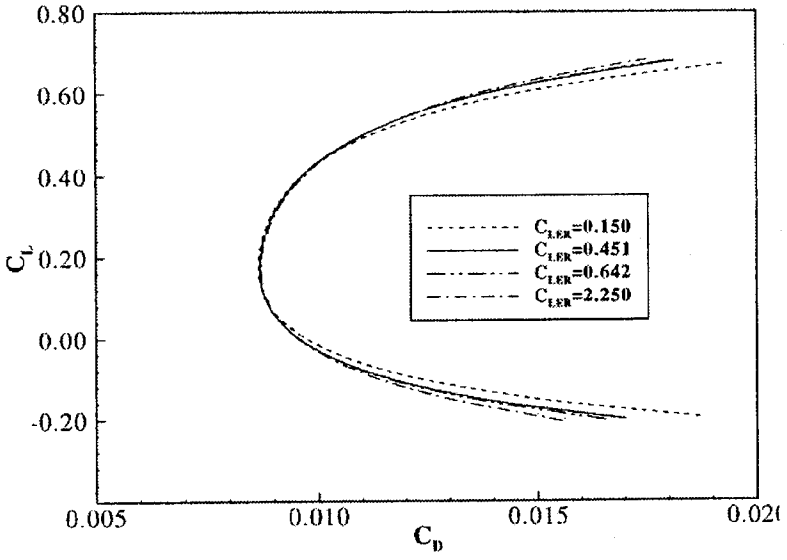

Figure 13. Comparison of lift-drag characteristics.

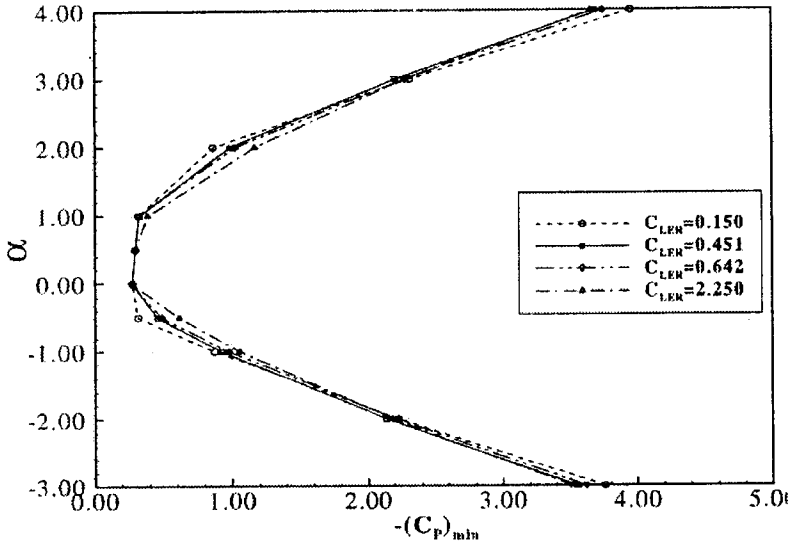

Figure 14. Minimum-pressure bucket diagrams.

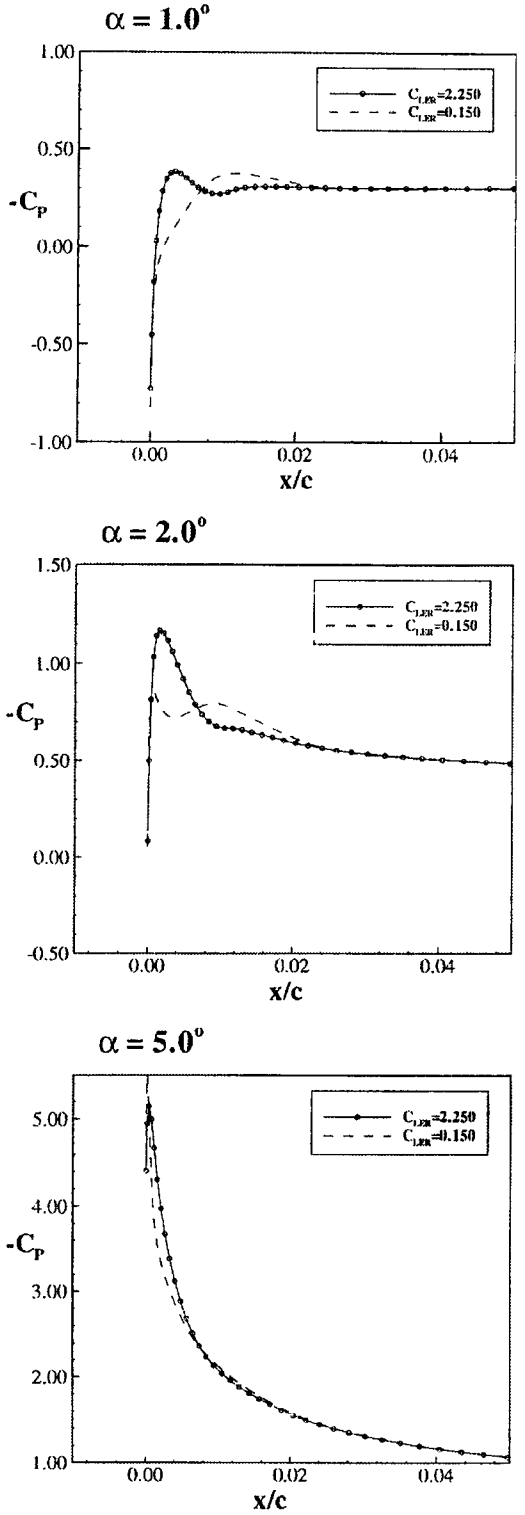

Figure 15. Pressure distribution near the leading edge.

Figure 14 shows minimum-pressure bucket diagrams for the foils with various leading edge radii, drawn from the minimum pressure values on the foil surface at various angles of attack. Near the ideal angle of attack of $0 < \alpha < 1.0°$, the minimum pressure point locates near the mid-chord and leading edge shape has no effects on the bucket diagram. As the angle of attack increases the minimum pressure location moves toward the leading edge and the effect of the leading edge shape on the bucket diagram becomes noticeable. The bucket diagram is wider for larger leading edge radius foils at larger attack angles of $\alpha > 3.0°$ and $\alpha < -2.0°$, which can be attributable to milder pressure distributions for the larger leading edge foil shapes.

Figure 15 shows pressure distributions near the leading edge on the suction side of the foils with different leading edge radii at (a) smaller angle of attack($\alpha = 1.0°$), (b) medium angle of attack($\alpha = 2.0°$), (c) larger angle of attack($\alpha = 5.0°$). Chordwise location of the negative pressure peak moves toward the leading edge as the angle of attack increases, where the movement of the smaller leading edge radius foil is faster. The peak values of the negative pressure of the smaller leading edge foil become larger than those of the larger leading edge foil, as the angle of attack increases.

The difference of the leading edge radius coefficient between 0.642 and 0.451 does not give much effects on the minimum-pressure bucket diagram. Since the value of 0.451 is more appropriate to draw and manufacture NACA66 sections and the change from 0.642 to 0.451 does not give noticeable differences in hydrodynamic characteristics, the value of the leading edge radius coefficient for NACA66 thickness form (TMB mod.) is selected as 0.451.

5 Conclusions

A RANS solver for two-dimensional foils was developed by adopting a finite volume method with an O-type grid system using the standard $k - \epsilon$ turbulence model. The developed code was validated by comparing the computed results for the Nakayama's foils with the available experimental results for the same foils. Effects of leading edge radii on the hydrodynamic performances of a NACA66 foil section were investigated by using the developed code.

Effect of leading edge radius on the lift-drag curve is relatively bigger at larger angle of attack conditions, where local pressure differences around the leading edge might have global effects on the lift and drag values. The foil with larger leading edge radius has smaller drag coefficient at the same lift coefficient, and as a result, exhibits a wider lift-drag curve.

Effect of leading edge radius on the minimum-pressure bucket diagrams was investigated. Near the ideal angle of attack condition detailed leading edge shapes do not influence the minimum-pressure bucket diagrams. As the angle of attack increases, the minimum pressure location moves toward the leading edge, and the effect of leading edge radius becomes noticeable. The bucket diagram is wider for larger leading edge radius foils at larger angles of attack.

The value of leading edge radius coefficient has been used as 0.642 at KRISO, since the NACA66 thickness form(TMB mod.) was introduced, where the value has been considered somewhat big. The value of 0.451 is considered to be more suitable to draw and manufacture NACA66 sections. Since the change of the leading edge radius coefficient from 0.642 to 0.451 does not give noticeable differences in the hydrodynamic characteristics of the foil, the leading edge radius coefficient for the NACA66 thickness form(TMB mod.) is recommended to be taken as 0.451.

Successful application of the developed code for the study of the leading edge radius suggests

that the code can be applied to the development of new blade sections having better hydrodynamic performances at wider angles of attack.

Acknowledgements

Support for this research was in part provided by MOST(Ministry of Science and Technology, Korea).

References

1. Nakayama, A., 1985, Characteristics of the Flow Around Conventional and Supercritical foils, J.F.M., Vol. 160.
2. Rhie, C. M., Chow, W. L., 1983, A Numerical Study of the Turbulent Flow Past an Isolated Airfoil with Trailing-Edge Separation, AIAA Journal, Vol.21.
3. Ahn, J.-W., Sung, H.-J., 1995, Prediction of Two-Dimensional Momentumless Wake by $k-\epsilon$ Model, AIAA Journal, Vol.33, No.4.
4. Van gunsteren, L. A., Pronk, C., 1973, Propeller Design Concept, Second LIPS Propeller Symposium, Holland.
5. Lee, J.-T., Ahn, J.-W. et. al., 1988, Development of High-Efficiency Propeller Series with New Blade Section, KRISO Report UCN160-1227-D.
6. Park, Y.-H., Kim, K.-S. et. al., 1998, The Influence of a Turbulence Stimulator on the Characteristics of 2-D hydrofoil, Proceedings of the Annual Meeting, The Society of Naval Architects of Korea.